Nuclear Science and Techniques (2026) 37:88
https://doi.org/10.1007/s41365-026-01883-9

Consequence assessment of plutonium aerosol diffusion after chemical explosion accident in an underground facility

Yong-Gang Huo[1] · Hong-Yi Yao[1] · Xing-Fu Cai[1] · Su-fen Li[1] · Fei Wang[1]

Received: 25 July 2024 / Revised: 20 September 2024 / Accepted: 28 September 2024 / Published online: 25 February 2026

Abstract
The aerosolization and diffusion of radioactive materials caused by chemical explosions represent a typical nuclear accident scenario that poses severe radioactive hazards to human health and the environment. This study examines the diffusion of plutonium aerosol generated by a chemical explosion within a typical representative underground facility. The state of explosion products following a single-point detonation of explosives was simulated. Subsequently, a numerical simulation of plutonium aerosol diffusion using the discrete phase model (DPM) was conducted based on the outcomes of the chemical explosion simulation. The simulation results indicate that plutonium aerosols diffuse throughout underground facilities after a chemical explosion; small particle size aerosols primarily accumulate in the upper part of the room after the accident; the concentrations of plutonium aerosol in the room and tunnel are significantly higher than those in the other areas; and the temporal variations in aerosol concentration in each area were quantified. Based on the particle concentration distribution and the effective dose computation approach, the study computes the internal irradiation dose received by personnel in seven areas over various time periods post-accident. Recommendations for emergency decision-making were derived from these calculations. These findings provide important theoretical insight and practical engineering application value for understanding the diffusion of radioactive aerosol in confined spaces following chemical explosions and for evaluating personnel radiation dose.

Keywords Plutonium · Aerosol diffusion · Underground facility · Internal irradiation dose · Chemical explosion

1 Introduction

The detonation of plutonium-encased explosives generates high temperature and pressure, leading to the aerosolization of plutonium and the formation of a radioactive smoke cloud. Inhalation of plutonium aerosol can cause internal irradiation, posing a significant and potentially fatal health hazard [1]. The diffusion of aerosol in a confined space following a chemical explosion occurs in two stages, namely the initial explosion and aerosol formation, followed by aerosol diffusion within the space. During the explosion stage, external forces are applied to the explosives to initiate a single-point detonation, creating a shockwave and aerosolizing the plutonium. The chemical energy is transformed into kinetic and thermal energy, producing a high-pressure wave and causing rapid radial diffusion of radioactive aerosol within milliseconds [2]. The radioactive smoke cloud expands and disperses due to airflow, resulting in environmental contamination and increased radioactive exposure. High doses of inhaled plutonium aerosol can cause severe acute internal irradiation sickness. Although plutonium operations are typically conducted underground, structural and ventilation challenges, along with aerosol distribution following explosions, complicate dose assessment and emergency response. The diffusion of plutonium aerosol in underground building settings (Fig. 1) underscores the critical need to analyze such environments, chemical explosions, and aerosol dose distribution.

In the field of chemical explosion research, Zhou used the Autodyn program to simulate the overpressure distribution of trinitrotoluene (TNT) explosions and compared the results with experimental data [3]. Liu et al. conducted numerical simulations and experimental studies based on the smoothed particle hydrodynamic (SPH) method to investigate the formation of radioactive aerosols resulting from

✉ Yong-Gang Huo
huoarmy@163.com

[1] Rocket Force University of Engineering, Xi'an 710025, China

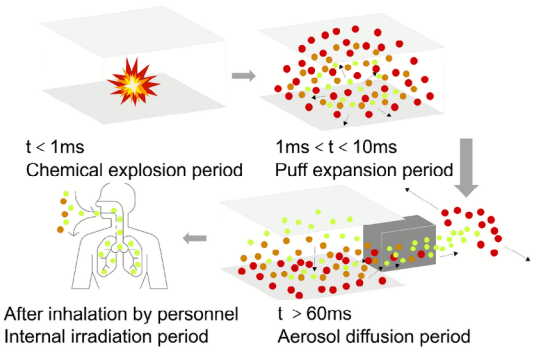

Fig. 1 (Color online) Schematic diagram of the aerosol dispersion process after a chemical explosion in a building

the fragmentation of uranium materials under explosive loads [4]. In the 1960s, the USA carried out the Operation Roller Coaster experiments, which focused on two main areas: characterizing plutonium detonation source terms and studying the atmospheric dispersion of plutonium aerosols. These experiments led to the development of nuclear accident aerosol dispersion models such as HOTSPOT, ERAD, and LODI [5–7]. Liu simulated the concentration distributions of ^{131}I, ^{85}Kr, and ^{137}Cs following a nuclear accident at a nuclear facility using the Lagrange smoke puff model [8]. Zhu et al. used Ventism software to numerically simulate the diffusion behavior of plutonium aerosol in complex underground chamber groups and provided ventilation recommendations [9]. Duan et al. used the HOTSPOT model to calculate and analyze the diffusion of radioactive aerosol after the chemical explosion of uranium-containing materials; however, due to the empirical nature of these models, discrepancies exist between predictions and actual outcomes [10]. Advances in hydrodynamic modeling have enabled more accurate simulations. Duan et al. applied a fluid dynamics model to simulate the rise of explosion smoke clouds, with experimental validation [11]. Mei et al. used a fluid–solid coupling simulation model to study the initial velocity and scattering behavior of powder materials in explosions [12]. The discrete phase model (DPM), an Euler–Lagrange mixture model, simulates particle motion in flow fields and enables precise calculation of particle forces and trajectories. Yuan et al. used the DPM to simulate the rise of particles produced by a 10 kg TNT explosive detonated in an open, windless environment [13]. Zhao et al. applied the DPM to assess dust explosion behavior in confined spaces [14]. Shuvalov et al. used the DPM to numerically simulate the formation and evolution of dust clouds generated by borehole blast explosions [15]. To address the problem of radioactive aerosol diffusion in confined spaces, Li investigated the migration and deposition of radioactive aerosol particles in air using direct numerical simulation combined with Lagrangian particle tracking and experimental measurements [16]. Yuan et al. analyzed the dispersion patterns of radioactive aerosol in an underground facility using fluid dynamics software and calculated personnel exposure doses [17]. Current literature shows that occupational exposure to plutonium aerosols significantly increases the risk of lung fibrosis in workers, a pathology observed in studies of Mayak plutonium workers and in animal models [18, 19]. Physiologically, early signs of lung fibrosis may appear within two months of exposure, while substantial lung damage can develop over 3 to 17 years. This does not diminish the serious health risks associated with plutonium aerosol exposure; rather, neglecting chronic effects and failing to provide appropriate medical intervention may result in severe long-term harm to exposed individuals. Consequently, assessing personnel exposure to plutonium aerosols is critically important.

Substantial international research has examined the diffusion of plutonium aerosol from chemical explosions, primarily using hydrodynamic models to analyze aerosol dispersion. However, limited research has focused on aerosol diffusion from chemical explosions in confined spaces and the corresponding personnel dose assessment. This research gap hinders accurate characterization of the spatial distribution of plutonium aerosol and reduces the effectiveness of emergency response guidance. In the event of a chemical explosion involving plutonium in an underground facility, plutonium may leak to the outside. Although individuals inside the facility would experience higher exposure levels than those outside, people outside are likely to be exposed to only a small fraction of the escaping aerosolized radioactive material, as they are farther from the accident site. Therefore, this study focuses exclusively on the effects of inhaling plutonium aerosols on individuals inside the facility.

In this study, we validated the feasibility of the DPM model for indoor particulate matter dispersion using existing experimental data. A numerical simulation of the chemical explosion process was then performed, incorporating results from the chemical explosion source term and plutonium aerosol parameters. Subsequently, we examined the diffusion of plutonium aerosol in a typical underground facility using the DPM model and analyzed the spatial distribution of plutonium aerosol following a chemical explosion. Based on the simulated spatial distribution of particle concentration and the dose coefficients from the International Commission on Radiological Protection (ICRP), the internal radiation dose received by individuals at different locations within the underground facility, without respiratory protection after the explosion, was calculated. These findings will provide technical support for emergency response efforts related to chemical explosion accidents involving radioactive materials.

2 Calculation models and parameters

2.1 Aerosol diffusion calculation model

The DPM model is a hybrid Eulerian–Lagrangian multiphase model. It treats the fluid and particles as the continuous phase and the discrete phase, respectively, determining the motion of the former by solving the Navier–Stokes equations and the motion of the latter by tracking particles in a Lagrangian coordinate system [20]. The DPM model is generally suitable for scenarios in which the volume fraction of the discrete phase is small.

$$\frac{\partial}{\partial t}(\alpha_g \rho_g) + \nabla \cdot (\alpha_g \rho_g \boldsymbol{v}_g) = 0, \tag{1}$$

$$\begin{aligned} &\frac{\partial}{\partial t}(\alpha_g \rho_g \boldsymbol{v}_g) + \nabla \cdot (\alpha_g \rho_g \boldsymbol{v}_g \boldsymbol{v}_g) = \\ &-\alpha_g \nabla p + \nabla \cdot (\bar{\boldsymbol{\tau}}_g) + \alpha_g \rho_g \boldsymbol{g} + K_{gs}(\boldsymbol{v}_p - \boldsymbol{v}_g), \end{aligned} \tag{2}$$

where α_g denotes the gas volume fraction; ρ_g represents the gas density; p signifies the pressure; $\boldsymbol{v}_g$ and $\boldsymbol{v}_p$ are the gas and particle velocities, respectively; t is the time; $\bar{\boldsymbol{\tau}}_g$ corresponds to the viscous stress term; $\boldsymbol{g}$ refers to the gravity vector; K_{gs} is the momentum exchange coefficient between the air and the particles; and ε denotes the dissipation rate of turbulent kinetic energy for the turbulence model.

$$m_s \frac{d\boldsymbol{v}_p}{dt} = m_s \frac{\boldsymbol{v}_g - \boldsymbol{v}_p}{\tau_r} + m_s \frac{g(\rho_s - \rho_g)}{\rho_s} + \boldsymbol{F}, \tag{3}$$

$$\tau_r = \frac{\rho_s d_s^2}{18\mu_g} \frac{24}{C_D Re_s}, \tag{4}$$

$$Re_s = \frac{\rho_g d_s |\boldsymbol{v}_p - \boldsymbol{v}_g|}{\mu_g}, \tag{5}$$

where m_s and ρ_s denote the particle mass and density, respectively; $m_s \frac{\boldsymbol{v}_g - \boldsymbol{v}_s}{\tau_r}$ signifies the drag force on the particle; $\boldsymbol{F}$ is the additional force, such as Saffman lift, thermophoretic force and other external forces which are different from gravity and drag force; τ_r represents the particle relaxation time; Re_s is the relative Reynolds number; d_s is the particle diameter; μ is the continuum phase viscosity; and C_D is the drag function.

The particle analysis report of plutonium aerosol from low-yield nuclear explosions in the former Soviet Union indicates that these aerosols can be approximated as spherical particles. Consequently, the spherical drag model is employed to characterize the drag force on plutonium aerosol [21]. The drag coefficient of plutonium aerosol is expressed as:

$$C_D = a_1 + \frac{a_2}{Re} + \frac{a_3}{Re^2}, \tag{6}$$

where a_1, a_2, and a_3 denote constants that vary with Re.

Saffman lift refers to the lift force acting on solid particles in a flow field with a velocity gradient, where particles in low-velocity regions move toward high-velocity regions. This additional force is significant for particles with low Reynolds numbers, such as submicron particles. Because plutonium aerosol from chemical explosions includes submicron particles, the Saffman lift needs to be considered. This study uses the expression proposed by Li et al. [22]:

$$\boldsymbol{F} = m_p \frac{2Kv^{1/2}\rho d_{ij}}{\rho_p d_p (d_{lk} d_{kl})^{1/4}} (\boldsymbol{v}_g - \boldsymbol{v}_p), \tag{7}$$

where K is a constant, d_{ij} denotes the deformation tensor, and v denotes the kinematic viscosity.

The thermophoretic force is the force exerted on particles in a gas due to a temperature gradient. During the aerosol diffusion phase, the substantial temperature difference between the smoke plume containing aerosol particles and the ambient air causes particle motion to be influenced by the thermophoretic force [23]. The thermophoretic force is defined as

$$\boldsymbol{F} = -D_{T,p} \frac{1}{T} \nabla T, \tag{8}$$

where $D_{T,p}$ denotes the thermophoretic coefficient.

2.2 Plutonium aerosol source term after chemical explosion

The chemical explosion radio-aerosol dispersion studies focus on determining aerosol source-term parameters, including plutonium aerosol particle density, particle size distribution, nuclide composition, aerosolization rate, and respirable fraction, which are critical inputs for numerical simulations of aerosol dispersion. Few experiments have established the source terms of plutonium aerosol under chemical explosion conditions. Data from the nonnuclear explosion of a plutonium-bearing device during ORC in 1964 in Nevada, USA, are particularly informative [24]. ORC included four experiments: Double Tracks (DT), Clean Slate 1 (CS1), Clean Slate 2 (CS2), and Clean Slate 3 (CS3). The DT experiment, involving a single-point detonation of plutonium-containing materials under uncovered conditions, most closely resembles the conditions of this study.

Aerosol measurements from the ORC DT experiment indicate that the average density of aerosol particles formed after a chemical explosion of plutonium is 4.9 g cm^{-3}. Luna et al. analyzed air-sampling data from air samples used during the ORC experiment to determine the particle size

distribution of plutonium aerosol [25]. Based on their findings, this study sets the particle size range for plutonium aerosol to 0.1 μm–120 μm, with the distribution following the Rosin–Rammler model.

The nuclide composition of weapons-grade plutonium materials was used to determine the nuclide composition and mass fraction of 1 kg of plutonium material [26]. Given the long half-lives of ^{239}Pu, ^{240}Pu, and ^{242}Pu, their decay products can be disregarded. Our study focuses on ^{234}U and ^{241}Am, produced by the decay of ^{238}Pu and ^{241}Pu. The quantities of ^{234}U and ^{241}Am are obtained from Eq. (9), and the radioactivity of different nuclides is determined from Eq. (10). Table 1 presents the nuclide composition, mass fraction, and radioactivity of nuclides released from 1 kg of plutonium material due to chemical explosions.

$$N_2^{(t)} = N_1^{(0)} \frac{\lambda_1 (e^{-\lambda_1 t} - e^{-\lambda_2 t})}{\lambda_2 - \lambda_1}, \tag{9}$$

$$A_i = \lambda_i N_i^{(0)}. \tag{10}$$

Plutonium aerosol primarily causes internal lung damage after inhalation [27]. In the ORC outfield experiments, plutonium materials exhibited a 100% aerosolization rate during chemical explosions, indicating that all of the plutonium was converted to aerosol. A respirable fraction (RF) of 16% was observed for DT, CS2, and CS3, and 20% for CS1 [28]. Based on these ORC experimental results, this study assumes a 100% aerosolization rate and a 20% respirable fraction for plutonium following a chemical explosion. The source-term parameters for the aerosol dispersion simulation are listed in Table 2.

2.3 Calculation method of internal irradiation dose caused by aerosol

Inhalation is the primary route for plutonium deposition in the human respiratory tract, with the extensive surface area of the alveoli facilitating the deposition of plutonium aerosol. Additionally, the plutonium aerosol produced by the explosion has limited solubility in the human body.

Table 2 Source-term parameters for plutonium aerosol following a chemical explosion

Plutonium aerosol source term	Settlement
Aerosol particle density	4.9 g cm^{-3}
Particle size distribution	0.1 μm–120 μm (Rosin-Rammler distribution)
Composition of nuclides	See Table 1
Aerosol rate	100%
Respirable fraction	20%

Because respirable aerosol particles are less than 10 μm, only the effective dose from inhalation of plutonium aerosol smaller than 10 μm is considered [29]. According to GB/T 16148-2009, the committed dose from inhaling a given radioactive aerosol is calculated as follows [30],

$$E(\tau) = A_0 e(\tau), \tag{11}$$

where A_0 denotes the radionuclide inhaled by the personnel and $e(\tau)$ is the effective dose coefficient corresponding to the radionuclide in Sv Bq^{-1}, which depends on the radionuclide's entry route into the human body, aerosol particle size, and the radionuclide form, as shown in Table 3.

$$A_0 = C_\mathrm{r} \cdot IR \cdot IP, \tag{12}$$

$$C_\mathrm{r} = \sum_j \frac{C_\mathrm{p}}{m_j} \cdot A_j, \tag{13}$$

where IR represents the respiration rate of the personnel; the nasal respiration rate during normal activity is 2.67×10^{-4} m^3 s^{-1}, and the respiration rate during exercise is 6.67×10^{-4} m^3 s^{-1} [31]; IP signifies the duration of inhalation in seconds; C_r is the activity concentration at a specific location in Bq m^{-3}; C_p refers to the plutonium aerosol particle concentration in the region in μg m^{-3}; m_j is the mass of the j-th plutonium isotope in the region in μg; A_j is the total activity of the j-th plutonium isotope in Bq.

Table 1 Mass and activity of nuclides released after a chemical explosion involving plutonium materials

Nuclide	Mass (g)	Mass fraction (%)	Half-life (a)	Total nuclide activity (Bq)
^{238}Pu	0.32	3.17×10^{-2}	87.74	2.00×10^{11}
^{239}Pu	9.33×10^{2}	93.80	2.40×10^{4}	2.15×10^{12}
^{240}Pu	59.80	6.01	6.50×10^{3}	4.93×10^{11}
^{241}Pu	1.48	0.15	15.20	5.63×10^{12}
^{242}Pu	0.40	4.02×10^{-2}	3.90×10^{5}	5.82×10^{7}
^{234}U	8.40×10^{-5}	8.00×10^{-6}	2.45×10^{5}	1.95×10^{4}
^{241}Am	9.86×10^{-4}	9.90×10^{-5}	432.20	1.25×10^{8}

Table 3 Effective dose coefficients for plutonium compounds

Effective dose coefficients (Sv Bq^{-1})				
Inhaled particulate materials (5 μm AMAD aerosols)	^{238}Pu	^{239}Pu	^{240}Pu	^{241}Pu
Plutonium dioxide, PuO_2, plutonium in mixed oxide	2.30×10^{-5}	2.50×10^{-5}	2.50×10^{-5}	4.40×10^{-7}

3 Numerical simulation of plutonium aerosol diffusion in underground structures

3.1 Simulation analysis of chemical explosion

The diffusion of aerosol following a chemical explosion in a confined space can be divided into two main stages. The first stage involves the chemical explosion and aerosol formation. The explosive material containing the plutonium is subjected to external forces, resulting in a single-point detonation. The resulting shock wave atomizes the plutonium metal under extremely high pressure and temperature. The energy released from the explosion is converted into kinetic and thermal energy, generating a high-pressure wave that violently disperses the radioactive aerosol radially. This process occurs on a microsecond timescale.

The second stage involves the spatial diffusion of the aerosol. The plutonium aerosol is carried by buoyant smoke and continues to diffuse until reaching a stable state. Due to the difficulty of experimentally observing the initial stage and the complexity of the associated physical and chemical processes, this study excludes the potential influence of plutonium materials on the chemical explosion process and assumes complete aerosolization of plutonium materials. Simulation calculations provide the spatial distributions of pressure, velocity, density, and temperature of the gas phase following the single-point detonation, forming the basis for constructing the aerosol diffusion source.

Assuming a TNT mass of 20 kg in a chemical explosion accident, the shock wave propagation following the chemical explosion is numerically simulated using Euler's finite difference method. The state of the explosion products is described using the Jones–Wilkins–Lee (JWL) equation of state and the ideal gas equation of state, with the JWL equation expressed as follows [32].

$$p = A\left(1 - \frac{\omega}{R_1 V}\right)e^{-R_1 V} + B\left(1 - \frac{\omega}{R_2 V}\right)e^{-R_2 V} + \frac{\omega e}{V}, \quad (14)$$

where p, V, and e denote the explosion product pressure, specific volume, and internal volumetric energy, respectively; A, R_1, R_2, and ω represent the JWL equation of state parameters.

Upon analyzing the spatial distribution of various explosion product parameters at different times, it is observed that at $t = 0.51$ ms, the shape of the shock wave transitions from spherical to hemispherical. The fireball then continues to expand in this form. The plutonium metal undergoes aerosolization and begins diffusing into the surrounding space. Figure 2 illustrates the spatial

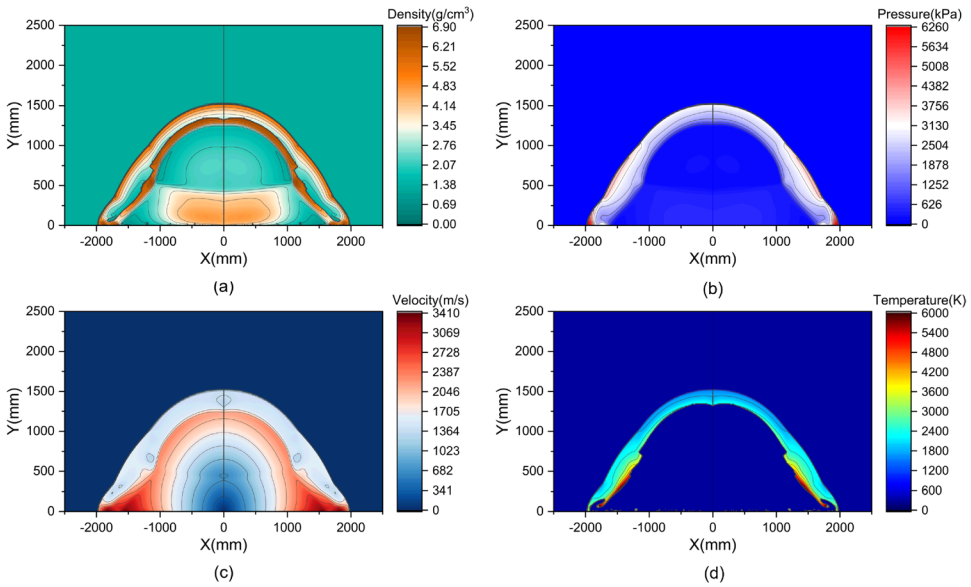

Fig. 2 (Color online) Spatial distribution of explosion product parameters at 0.51ms after the chemical explosion: **a** spatial distribution of density, **b** spatial distribution of pressure, **c** spatial distribution of velocity magnitude, and **d** spatial distribution of temperature

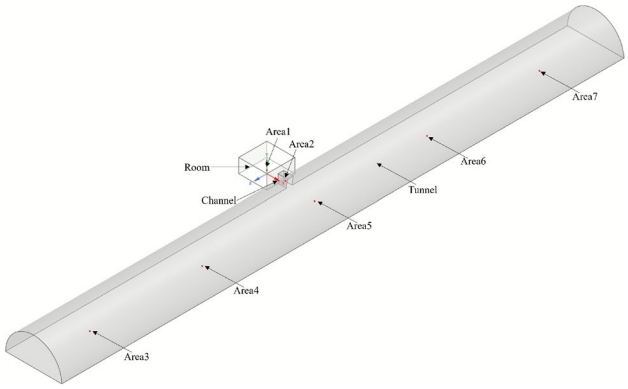

Fig. 3 (Color online) Typical underground facility model

distribution of the explosion product parameters at 0.51 ms, revealing a distinct double-layer structure. This structure consists of an inner layer characterized by a negative-pressure environment and an outer layer exhibiting overpressure conditions.

3.2 Simulation scene construction

A typical underground facility structure with an operation room and a tunnel is selected for analysis, as illustrated in Fig. 3. The ground center of the room is assumed to be the location of the chemical explosion accident. The room measures 10 m × 10 m × 5 m, and the channel connecting the room to the tunnel is 3 m in length with a cross section of 2 m × 3 m. The tunnel is 200 m in length and has a semicircular cross-sectional area with a diameter of 20 m. The wall-jet model is employed as the ground boundary condition for the underground facility, and the reflect model is applied to the walls, considering the inviscid nature of plutonium aerosol particles. It is assumed that the explosion results in the channel becoming open after the accident, and that no directional ventilation is performed in the underground facility. The ambient pressure before the accident is taken as the standard atmospheric pressure.

The coordinate origin is placed at the center of the room's floor. Seven monitoring areas are established to support subsequent monitoring of aerosol parameters. The monitoring area is defined based on the hemispherical breathing zone specified by the US Department of Labor, which encompasses the area in front of the shoulders of personnel [33]. This breathing zone is approximately 6–9 in. As the orientation of personnel is unknown, the monitoring zones are defined as spheres with a radius of 1.2 m. The coordinates of the spherical center of each monitoring area are listed in Table 4.

Table 4 Monitoring point configuration

	Coordinates of monitoring domain center
Area 1	(0,1.2,0)
Area 2	(6.5,1.2,0)
Area 3	(18,1.2,80)
Area 4	(18,1.2,40)
Area 5	(18,1.2,0)
Area 6	(18,1.2,–40)
Area 7	(18,1.2,–80)

3.3 Simulation of plutonium aerosol diffusion of chemical explosion

After the chemical explosion, plutonium aerosol initially diffuses in a hemispherical radial pattern within the room due to the strong shock wave. The particles then rapidly enter the tunnel through the channel and, because of their high initial velocity, continue to diffuse and spread toward both ends of the channel after colliding with the tunnel wall. The simulation results analyze the particle size, particle velocity, air density, particle number, mass fraction in space, and particle concentration at different positions.

3.3.1 Spatial distribution of plutonium aerosol

Figure 4a shows the radial distribution of aerosol particles in the room at 0.01 s following the chemical explosion, with larger particles diffusing at a faster rate. Figure 4b illustrates the rapid influx of aerosol particles into the tunnel, driven by the substantial pressure and density differential between the puff interior and the surrounding environment. Figure 4c and d depicts the diffusion behavior of aerosol particles upon collision with the tunnel wall, leading to their distribution toward both ends. As the particles decelerate due to the wall impact, their velocity decreases during the diffusion process until the aerosol state in the environment reaches equilibrium.

Figure 5a and b shows that after 300 s, most aerosol particles are concentrated at both ends of the tunnel, with particle velocity reduced to below 1 m s^{-1}. In Fig. 5c, significant layering of particles within the tunnel is evident at 600 s. Particles in the upper layer diffuse slowly to both ends at a velocity of less than 0.15 m s^{-1}, while a small number of particles continue to migrate into the tunnel through the channel.

3.3.2 Plutonium aerosol concentration distribution

By establishing monitoring zones within the reference person's breathing area at various locations (Table 4), this study

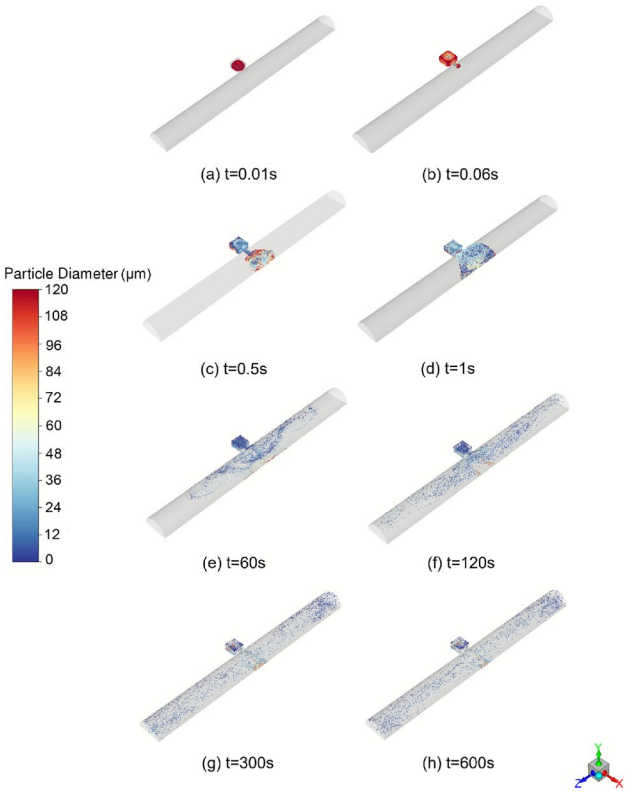

Fig. 4 (Color online) Spatial distribution of plutonium aerosol of various particle sizes at different points in time

observed fluctuations in particle concentration within these zones 10–600 s after the accident. These observations were used to determine the internal irradiation dose received by subsequent personnel from inhaling plutonium aerosol.

As shown in Fig. 6, in Area 1, particle concentrations remained above 100 μg m^{-3} before 200 s, gradually declining thereafter. A sharp decrease below 10 μg m^{-3} occurred between 200 s and 250 s, followed by a slow decline to approximately 1 μg m^{-3} after 250 s. Area 2 exhibited a decrease to 100 μg m^{-3} at approximately 150 s, followed by a rapid increase peaking at about 300 s, and subsequently decreasing rapidly to 1 μg m^{-3} after 400 s. As illustrated in Fig. 7, the concentration trends in Areas 3 and 7 mirrored each other, starting near zero before 180 s, rising to approximately 5 μg m^{-3} at 200 s, and subsequently decreasing. A secondary rise occurred around 250 s, peaking at about 11 μg m^{-3} at 300 s, and then decreasing between 300 s and 600 s, with minor fluctuations observed between 350 s and 450 s. Areas 4 and 6 show similar trends, peaking initially at 70 s, dropping to 0, and subsequently rising again to a maximum of 10 μg m^{-3} at 300 s, gradually decreasing to 0. Area 5 peaked at 13.5 μg m^{-3} at 30 s, declining to near zero between 30 s and 190 s, with a second peak reaching 9 μg m^{-3}at 300 s before gradually declining again to near zero between 300 s and 600 s. The internal irradiation dose received by personnel in an accident area is directly linked to the mass of plutonium aerosol inhaled in that area. This mass can be determined by computing the plutonium aerosol concentration at different inhalation times.

3.4 Assessment of internal irradiation dose to personnel

The internal irradiation dose received by personnel near the chemical explosion accident site correlates with the mass of plutonium aerosol inhaled in that area. The mass of plutonium aerosol inhaled at different times can be determined by computing the concentration of plutonium aerosol during the initial stages of the incident. Because personnel are most affected shortly after the explosion, only the internal irradiation of individuals at various locations after 5 s of the chemical explosion is considered. The effective doses received by personnel in each monitoring area over different time periods are provided in Tables 5 and 6.

The variation in effective doses across regions over different time periods closely corresponds to changes in particle concentration in those regions. The decision to remain in Area 2 is likely influenced by the considerable internal exposure risk. First, because the channel serves

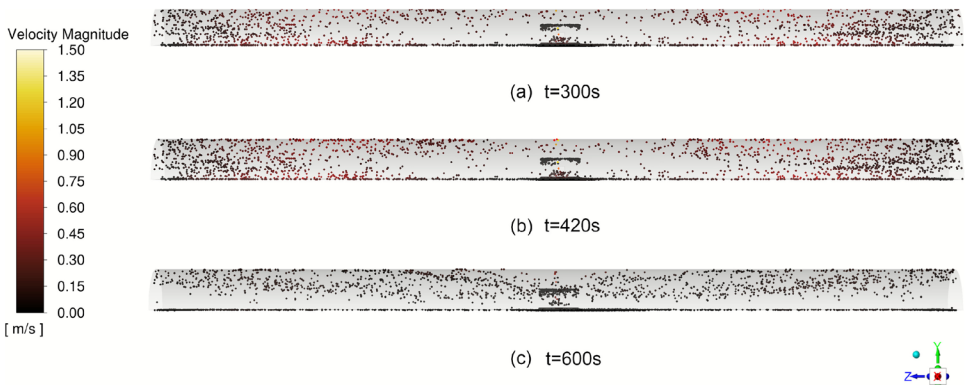

Fig. 5 (Color online) Plutonium aerosol velocity distribution at different points in time

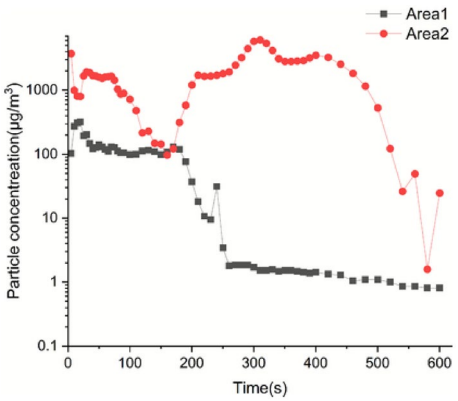

Fig. 6 (Color online) Plutonium aerosol concentrations in Areas 1 and 2 as a function of time

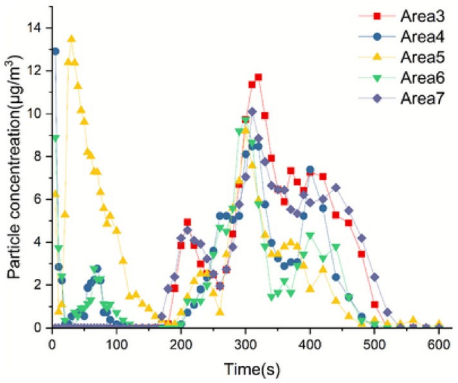

Fig. 7 (Color online) Plutonium aerosol concentrations in Areas 3–7 as a function of time

as the passage between the room and the tunnel, any outward diffusion of plutonium aerosol must pass through this area. Second, the low channel height restricts the movement of smaller particle size plutonium aerosol particles, which tend to accumulate at higher positions in space. This constraint increases the likelihood that these particles will be present at a person's breathing height.

According to data reported by Giardina, the settlement velocity of 5 μg m^{-3} aerosol particles within a confined space is 0.002 m s^{-1}, ensuring that small particles at breathing height settle within one hour after a chemical explosion [34]. Simulation results (Tables 5 and 6) for plutonium aerosol diffusion show clear stratification at 600 s, with the horizontal velocity becoming negligible. Therefore, gravity deposition is the primary factor to consider [35]. It can be assumed that the internal radiation dose received by subsequent personnel is consistent with the computed results between 540 s and 600 s. The effective dose at each monitoring point within one hour can thus be estimated, as shown in Tables 7 and 8. As indicated by the estimates presented in these tables, the likelihood of inhalation of plutonium aerosols and internal exposure of personnel in the various areas 10 min after the accident is markedly reduced. In particular, the cumulative dose increase in Areas 4 and 6 is nearly negligible, at less than 0.01%.

According to ICRP recommendations, a brief exposure to an internal radiation dose exceeding 250 mSv surpasses the emergency dose threshold, potentially causing irreversible damage and significantly increasing the incidence of lung cancer [36]. Newman et al. showed that the risk of pulmonary fibrosis increased sharply when the lung dose exceeded 10 Sv [18].

The estimated internal irradiation dose to personnel may be higher in the rooms and channels than that in other regions. If personnel enter the room within 240 s after an accident and stay there for more than a minute, they are likely to receive a dose exceeding 250 mSv. Even after 540 s, traversing the channel can cause lung damage. While the estimated cumulative internal irradiation dose to personnel in other areas may not reach the threshold, increased respiratory rates and the resuspension of ground-deposited aerosols owing to the movement of personnel could

Table 5 Internal irradiation dose to personnel in each monitoring area at different time intervals at a respiration rate of 2.67×10^{-4} m^3 s^{-1}

Internal irradiation dose (mSv)							
Time (s)	Area 1	Area 2	Area 3	Area 4	Area 5	Area 6	Area 7
5–60	185.64	1458.90	0.00	0.93	8.65	0.94	0.00
60–120	128.89	1116.29	0.00	1.08	5.87	1.38	0.00
120–180	133.48	197.68	0.02	0.00	1.04	0.02	0.29
180–240	44.52	1542.02	3.71	0.98	1.65	0.98	4.27
240–300	1.95	3117.44	4.28	5.21	4.31	5.99	3.73
300–360	1.49	3915.10	8.75	5.32	4.47	3.56	7.45
360–420	1.37	3155.22	6.83	5.20	2.76	3.32	5.71
420–480	0.88	1443.16	3.62	1.14	0.50	1.38	5.71
480–540	0.77	157.20	0.22	0.00	0.18	0.04	0.76
540–600	0.64	15.14	0.00	0.00	0.11	0.00	0.01

Table 6 Internal irradiation dose to personnel in each monitoring area at different time intervals at a respiration rate of 6.67×10^{-4} m^3 s^{-1}

Internal irradiation dose (mSv)							
Time (s)	Area 1	Area 2	Area 3	Area 4	Area 5	Area 6	Area 7
5–60	464.10	3647.24	0.00	2.32	21.62	2.36	0.00
60–120	322.22	2790.72	0.00	2.71	14.67	3.46	0.00
120–180	333.71	494.20	0.06	0.00	2.59	0.04	0.72
180–240	111.30	3855.05	9.27	2.44	4.13	2.45	10.67
240–300	4.86	7793.61	10.70	13.04	10.78	14.98	9.32
300–360	3.72	9787.74	21.87	13.30	11.18	8.90	18.62
360–420	3.43	7888.06	17.09	12.99	6.89	8.30	14.26
420–480	2.19	3607.91	9.06	2.84	1.24	3.45	14.26
480–540	1.93	393.00	0.55	0.00	0.44	0.09	1.89
540–600	1.61	37.84	0.00	0.00	0.27	0.00	0.01

Table 7 Estimated cumulative dose in each region at different times at a respiration rate of 2.67×10^{-4} m^3 s^{-1}

Internal irradiation dose (mSv)							
Time (min)	Area 1	Area 2	Area 3	Area 4	Area 5	Area 6	Area 7
5	494.47	7432.32	8.01	8.20	21.52	9.31	8.28
10	499.63	16118.15	27.44	19.86	29.53	17.61	27.90
15	502.84	16193.83	27.44	19.86	30.07	17.61	27.93
30	512.47	16420.89	27.46	19.86	31.69	17.61	29.00
60	531.73	16874.99	27.50	19.86	34.95	17.61	28.14

Table 8 Estimated cumulative dose in each region at different times at a respiration rate of 6.67×10^{-4} m^3 s^{-1}

Internal irradiation dose (mSv)							
Time (min)	Area 1	Area 2	Area 3	Area 4	Area 5	Area 6	Area 7
5	1236.19	18580.81	20.03	20.50	53.79	23.28	20.71
10	1249.06	40295.37	68.59	49.64	73.82	44.02	69.76
15	1257.09	40484.58	68.61	49.64	75.17	44.02	69.82
30	1281.16	41052.21	68.65	49.64	79.24	44.02	69.99
60	1329.32	42187.48	68.74	49.64	87.37	44.02	70.34

increase the actual internal irradiation dose beyond the estimated value presented in this paper.

Based on the results of the previous simulation, the following emergency response recommendations were proposed for this type of accident involving a plutonium-containing explosion in a confined space. Respondents should avoid entering the area within 10 min of the accident because of the high concentration of plutonium aerosols at breathing height. If entering an area is necessary, appropriate respiratory protection should be provided to prevent the inhalation of plutonium aerosols. Avoid Areas 1 and 2, where the concentration of plutonium aerosols at breathing height is significantly higher than in other areas. For people in the danger zone at the time of the accident, the following evacuation recommendations may help reduce the risk of inhaling plutonium aerosols: move as low as possible, as simulation results show that inhalable plutonium aerosols tend to rise and concentrate above the room during the early stages of the accident; cover the nose and mouth with clothing (such as a T-shirt or cloth) to filter some of the aerosol; although this is not a substitute for professional respiratory protection, it may reduce the amount of plutonium inhaled to some extent; move to the nearest emergency exit as quickly as possible, but calmly, to avoid panic-induced increases in respiratory rate. In similarly confined spaces, the installation of an air suction system can also rapidly reduce the aerosol concentration in a facility following such incidents.

4 Summary

This study addresses the issue of internal irradiation of personnel resulting from the plutonium aerosol diffusion following chemical explosions in underground facilities. We initially simulated the aftermath of a 20 kg TNT explosion using the JWL equation. Next, a model was developed to

simulate the release of 1 kg of plutonium aerosol. Subsequently, the plutonium aerosol diffusion process was simulated using the DPM model to analyze the spatial and concentration distributions. Internal irradiation doses to personnel in seven areas were computed for different time periods after the accident using the effective dose calculation method, and emergency recommendations were formulated based on these calculation results. Simulation results indicate that a plutonium aerosol-containing smoke cloud forms after the chemical explosion, rapidly expanding within the room and infiltrating the tunnel via the channel due to the significant pressure and density disparities between the smoke cloud and the surrounding environment. The cloud then diffuses toward both ends. Larger particles settle rapidly under gravity, whereas smaller particles remain suspended, forming a stratified layer over time. Plutonium aerosol concentrations were substantially higher in the room and channel than in other areas, corresponding to higher internal irradiation doses to personnel in these locations. Personnel health risks were assessed by modeling and estimating the internal exposure doses due to inhalation within the facility. The results show that prolonged occupancy in the affected areas places personnel at increased risk of lung fibrosis. Based on these findings, emergency recommendations were developed. This study employs multiple computational models to analyze the plutonium aerosol diffusion process and associated internal irradiation risks associated with chemical explosions in confined underground facilities. These findings provide essential theoretical support for developing effective emergency response strategies to mitigate such incidents.

Author contributions All authors contributed to the study conception and design. Numerical simulation and data collection and analysis were performed by Xing-Fu Cai, Su-fen Li, and Fei Wang. The first draft of the manuscript was written by Yong-Gang Huo and Hong-Yi Yao; all authors commented on previous versions of the manuscript. All authors read and approved the final manuscript.

Data availability The data that support the findings of this study are openly available in Science Data Bank at https://cstr.cn/31253.11.sciencedb.j00186.00801 and https://www.doi.org/10.57760/sciencedb.j00186.00801.

Declarations

Conflict of interest The authors declare that they have no conflict of interest.

References

1. E.J. Chatfield, The generation of particulate aerosol from plutonium surfaces. Atmos. Environ. **2**, 97–101 (1968). https://doi.org/10.1016/0004-6981(68)90025-5
2. W.J. Liu, Q.P. Ma, L.Z. Tian et al., Experimental simulation of aerosol source term of surrogate plutonium produced by high-explosive detonation. Acta Armament. **37**, 447–454 (2016). https://doi.org/10.3969/j.issn.1000-1093.2016.03.009. (**in Chinese**)
3. B.S. Zhou, L.H. Zhang, S.L. Wang et al., Numerical simulation and experimental research on TNT explosion shock wave. J. Proj. Rock. Miss. Guid. **30**, 88–90 (2010). https://doi.org/10.15892/j.cnki.djzdxb.2010.03.023. (**in Chinese**)
4. Z.Y. Liu, J.T. Wang, B. He et al., Study on the formation mechanism of uranium aerosol under explosion load. Explos. Shock Waves **41**, 052201 (2021). https://doi.org/10.11883/bzycj-2021-0075. (**in Chinese**)
5. S.G. Homann, HOTSPOT health physics codes for the PC. Lawrence Livermore National Lab. (LLNL), Livermore, CA (United States), (1994)
6. B.A. Boughton, J.M. DeLaurentis, Description and validation of ERAD: an atmospheric dispersion model for high explosive detonations. Sandia National Lab. (SNL-NM), Albuquerque, NM (United States), (1992)
7. J.S. Nasstrom, G. Sugiyama, R.L. Baskett et al., The national atmospheric release advisory center modelling and decision-support system for radiological and nuclear emergency preparedness and response. Int. J. Emerg. Manag. **4**, 524–550 (2007). https://doi.org/10.1504/IJEM.2007.014301
8. S. Liu, *Simulation Study on Diffusion of Airborne Radioactive Contaminants in Nuclear Accident* (Harbin Engineering University, 2017). (**in Chinese**)
9. Y. Zhu, H. Zhou, H.Y. Zhao et al., Diffusion behavior of plutonium aerosol in nuclear accidents in complex underground chamber group. Saf. Environ. Eng. **30**, 96–105 (2023). https://doi.org/10.13578/j.cnki.issn.1671-1556.20220970. (**in Chinese**)
10. Z.S. Duan, Y.F. Luo, W. Yuan et al., The aftereffect forecast and analysis for accidents of uranium explosive. Nucl. Electron. Detect. Technol. **31**, 90–94 (2011). https://doi.org/10.3969/j.issn.0258-0934.2011.01.022. (**in Chinese**)
11. Z.S. Duan, H.P. Guo, X.J. Feng et al., Space-time distribution model and characteristics of explosion cloud diffusion. Explos. Shock Waves **39**, 054202 (2019). https://doi.org/10.11883/bzycj-2017-0380. (**in Chinese**)
12. Z. Mei, P. Chen, J. Liu, Numerical analysis of initial cloud of powder dynamic dispersion. J. Phys. Conf. Ser. **2478**, 022013 (2023). https://doi.org/10.1088/1742-6596/2478/2/022013
13. T. Yuan, Y.F. Luo, A.G. Shang et al., Numerical study on particle motion in explosion buoyant puff. Explos. Shock Waves **33**, 556–560 (2013). https://doi.org/10.3969/j.issn.1001-1455.2013.05.017. (**in Chinese**)
14. Y. Zhao, R.P.K. Ambrose, Predicting continuous dispersion and deposition of explosive dust in confined spaces using a discrete phase model. Powder Technol. **408**, 117704 (2022). https://doi.org/10.1016/j.powtec.2022.117704
15. V. Shuvalov, V. Khazins, A. Krasheninnikov et al., Formation and evolution of a dust cloud as a result of TNT detonation in a borehole: Numerical simulation. Mining **3**, 261–270 (2023). https://doi.org/10.3390/mining3020016

16. Y. Li, *Study on the Loss Mechanism of Radioaerosol during the Transportation in the Containment* (Shanghai Jiao Tong University, 2018). https://doi.org/10.27307/d.cnki.gsjtu.2018.000482 (**in Chinese**)
17. W. Yuan, L. Zuo, X.B. Chen et al., Study on the diffusion of aerosol in underground military building when nuclear accident happen. Sci. Tech. Eng. **13**, 8455–8459 (2013). https://doi.org/10.3969/j.issn.1671-1815.2013.28.043. (**in Chinese**)
18. L.S. Newman, M.M. Mroz, A.J. Ruttenber, Lung fibrosis in plutonium workers. Radiat. Res. **164**, 123–131 (2005). https://doi.org/10.1667/rr3407
19. J. Grellier, W. Atkinson, P. Bérard et al., Risk of lung cancer mortality in nuclear workers from internal exposure to alpha particle-emitting radionuclides. Epidemiology **28**, 675–684 (2017). https://doi.org/10.1097/EDE.0000000000000684
20. S.A.J. Morsi, A.J. Alexander, An investigation of particle trajectories in two-phase flow systems. J. Fluid Mech. **55**, 193–208 (1972). https://doi.org/10.1017/S0022112072001806
21. Y.S. Cheng, R.A. Guilmette, Y. Zhou et al., Characterization of plutonium aerosol collected during an accident. Health Phys. **87**, 596–605 (2004). https://doi.org/10.1097/01.hp.0000138577.21388.a7
22. A. Li, G. Ahmadi, Dispersion and deposition of spherical particles from point sources in a turbulent channel flow. Aerosol Sci. Technol. **16**, 209–226 (1992). https://doi.org/10.1080/02786829208959550
23. R. Piazza, Thermophoresis: moving particles with thermal gradients. Soft Matter **4**, 1740–1744 (2008). https://doi.org/10.1039/B805888C
24. W.J. Liu, B.Y. Hu, Q.Z. Li, Review of plutonium aerosol source term in nuclear accident. J. Saf. Environ. **11**, 259–263 (2011). https://doi.org/10.3969/j.issn.1009-6094.2011.05.058. (**in Chinese**)
25. R.E. Luna, H.W. Church, J.D. Shreve, Variability of air sampler data. Atmos. Environ. **5**, 579–597 (1971). https://doi.org/10.1016/0004-6981(71)90114-4
26. X.H. Tang, N. Yang, L.H. Bao et al., Numerical simulation of aerosol dispersion with the explosive's detonation in the process of nuclear weapon transportation. J. Saf. Environ. **14**, 142–148 (2014). https://doi.org/10.13637/j.issn.1009-6094.2014.01.034. (**in Chinese**)
27. B. Xie, X.G. Long, A review of plutonium aerosol research in some American national laboratories. Sci. Technol. Rev. **35**, 115–124 (2017). https://doi.org/10.3981/j.issn.1000-7857.2017.21.014. (**in Chinese**)
28. C.Y. Xie, J.R. Luo, L.L. Guo, Study on the diffusion of aerosol released by the explosion of explosives. China Saf. Sci. J. **18**, 87–91 (2008). https://doi.org/10.3969/j.issn.1003-3033.2008.10.015. (**in Chinese**)
29. S.A. Romanov, A.V. Efimov, E.E. Aladova et al., Plutonium production and particles incorporation into the human body. J. Environ. Radioact. **211**, 106073 (2020). https://doi.org/10.1016/j.jenvrad.2019.106073
30. Q.F. Liu, Q. Liu, Q. Wu et al., Specification for assessment of intakes and internal doses of radionuclides, GB/T 16148-2009, General Administration of Quality Supervision, (2009) (in Chinese)
31. J.D. Pleil, M.A.G. Wallace, M.D. Davis et al., The physics of human breathing: flow, timing, volume, and pressure parameters for normal, on-demand, and ventilator respiration. J. Breath Res. **15**, 042002 (2021). https://doi.org/10.1088/1752-7163/ac2589
32. Y.J. Wang, S.D. Zhang, H. Li et al., Uncertain parameters of Jones-Wilkins-Lee equation of state for detonation products of explosive. Acta Phys. Sin. **65**, 106401 (2016). https://doi.org/10.7498/aps.65.106401. (**in Chinese**)
33. Occupational Safety and Health Administration, Ethylene oxide (EtO): Understanding OSHA's exposure monitoring requirements (2007), https://www.osha.gov/sites/default/files/publications/OSHA_ethylene_oxide.pdf
34. M. Giardina, P. Buffa, A new approach for modeling dry deposition velocity of particles. Atmos. Environ. **180**, 11–22 (2018). https://doi.org/10.1016/j.atmosenv.2018.02.038
35. A.H. Liu, *The Calculation Study of the Concentration and the Radiation Dose of Airborne Radionuclides from Nuclear Facility* (Shanghai Jiao Tong University, 2012). (**in Chinese**)
36. M.W. Charles, ICRP publication 103: recommendations of the ICRP. Radiat. Prot. Dosim. **129**, 500–507 (2008). https://doi.org/10.1093/rpd/ncn187